HHS Public Access

Author manuscript

Neuron. Author manuscript; available in PMC 2018 May 30.

Published in final edited form as:

Neuron. 2017 December 06; 96(5): 1099–1111.e3. doi:10.1016/j.neuron.2017.09.058.

'Silent' NMDA synapses enhance motion sensitivity in a mature retinal circuit

Santhosh Sethuramanujam[1], **Xiaoyang Yao**[2], **Geoff deRosenroll**[1], **Kevin L. Briggman**[3], **Greg D. Field**[2], and **Gautam B. Awatramani**[1,4]

[1]Department of Biology, University of Victoria, Victoria, BC V8W 3N5, Canada

[2]Department of Neurobiology, Duke University School of Medicine, Durham, United States

[3]Department of Computational Neuroethology, Center of Advanced European Studies andResearch (caesar), 53175 Bonn, Germany

Summary

Retinal direction-selective ganglion cells (DSGCs) have the remarkable ability to encode motion over a wide range of contrasts, relying on well-coordinated excitation and inhibition (E/I). E/I is orchestrated by a diverse set of glutamatergic bipolar cells that drive DSGCs directly, as well as indirectly through feed-forward GABAergic/cholinergic signals mediated by starburst amacrine cells. Determining how direction-selective responses are generated across varied stimulus conditions requires understanding how glutamate, acetylcholine and GABA signals are precisely coordinated. Here, we use a combination of paired patch-clamp recordings, serial EM and large-scale multi-electrode array recordings to show that a single high-sensitive source of glutamate is processed differentially by starbursts via AMPA receptors and DSGCs via NMDA receptors. We further demonstrate how this novel synaptic arrangement enables DSGCs to encode direction robustly near threshold contrasts. Together, these results reveal a space-efficient synaptic circuit model for direction computations, in which 'silent' NMDA receptors play a critical roles.

Introduction

Synapses lacking the functional expression of AMPA receptors are often considered 'silent' (Kerchner and Nicoll, 2008), as glutamate binding to NMDA receptors alone does not substantially activate them (due to their voltage-dependent block of NMDA receptors by external Mg^{2+} ions). Studies over the past two decades have established silent synapses as prominent cellular substrates for synaptic plasticity in the developing brain (reviewed by Kerchner and Nicoll, 2008). However, their unique dependency of two simultaneous conditions—presynaptic glutamate release and postsynaptic depolarization—also make

Correspondence should be addressed to: Dr. Gautam Awatramani, Department of Biology, 259D Cunningham, University of Victoria, Victoria, BC V8W 3N5, Phone: 250-472-5178, gautam@uvic.ca.

[4]Lead contact

Author Contributions: Conceptualization, S.S., G.D, G.D.F and G.B.A.; Methodology, G.F., K.B. and G.B.A.; Investigation, S.S. carried out the whole-cell patch-clamp recordings; K.B. analyzed the SBEM data set; G.D. constructed the NEURON models; X.Y. performed and analyzed the MEA recordings; Writing - Original Draft, S.S., G.D.F. and G.B.A.; Writing -Review & Editing, S.S., X.Y., G.D., G.D.F, K.B and G.B.A.; Funding Acquisition, G.F, K.B and G.B.A.; Resources, G.D.F, K.B and G.B.A.; Supervision, G.D.F, K.B and G.B.A.

NMDA-dominated synaptic pathways an attractive candidate for mediating silent modulatory signals observed in mature brain (Herrero et al., 2013; Rivadulla et al., 2001; Self et al., 2012; Shima and Tanji, 1998; Wang, 2001). For example, elegant *in vivo* pharmacological studies demonstrate that the modulatory effects of covert attention signals on the responsiveness of neurons in the visual cortex are abolished when NMDA receptors are antagonized (Herrero et al., 2013; Self et al., 2012). However, there is little direct evidence for silent synapse expression in the mature CNS (reviewed by Hanse et al., 2013; Kerchner and Nicoll, 2008), and the synaptic mechanisms by which they enhance neural computations remain unexplored.

Assessing the contributions of silent NMDA receptor-dominated pathways to neural computation is difficult because these pathways are poorly defined and intermingled with other excitatory pathways, such as those driven by AMPA receptors and/or non-glutamatergic receptors. Interestingly, in the direction-selective (DS) retinal circuit that we examine here, we recently observed that under cholinergic receptor blockade, bipolar cell glutamate inputs to ON-OFF DS ganglion cells (DSGCs; output neurons that relay directional information from retina to higher visual centers) evoked by low-contrast stimuli were mediated by silent NMDA synapses (Sethuramanujam et al., 2016). The AMPA receptor-mediated component of the DSGC's synaptic response only appeared at higher stimulus contrasts. In contrast, however, a number of other studies indicate that AMPA/NMDA receptor-mediated inputs to DSGCs scale together as a function of contrast, consistent with observations in other types of ganglion cells, suggesting that AMPA and NMDA receptors are driven by a common source of glutamate (Buldyrev et al., 2012; Diamond and Copenhagen, 1995; Manookin et al., 2010; Poleg-Polsky and Diamond, 2016b; Stafford et al., 2014). These diverging results have given rise to two distinct models that explain how the DS circuit coordinates inhibition/excitation over a range of stimulus contrasts (Figure 1A & D), which underlies the DSGC's robust ability to compute direction (Grzywacz and Amthor, 2007; Nowak et al., 2011; Poleg-Polsky and Diamond, 2016b).

In the conventional model, DSGCs compute direction by comparing the relative strength of non-directional bipolar cell inputs mediated by AMPA/NMDA receptors with highly directional starburst inputs mediated by $GABA_A$ receptors (reviewed by Mauss et al., 2017; Vaney et al., 2012). In this model, changing the strength of bipolar cell input relative to inhibition strongly affects the tuning properties of DSGCs. Thus, maintaining DS tuning properties over a range of contrasts requires glutamate, GABA and ACh signals to DSGCs to scale proportionally as a function of contrast (Figure 1B). To achieve such presynaptic balance, glutamate release from bipolar cells onto DSGCs must be curbed until stimuli are sufficiently strong to evoke GABA release from starbursts. This is thought to be accomplished by using high- and low-sensitivity bipolar cells (Ichinose et al., 2014; Odermatt et al., 2012; Poleg-Polsky and Diamond, 2016b) to independently drive starbursts and DSGCs, in a way that compensates for the starburst's threshold non-linearity (Figure 1A & B) (Poleg-Polsky and Diamond, 2016b). As this model requires the matching of presynaptic GABA/glutamate/ACh signals, we refer to it as the ‘matched’ model for DS in ganglion cells.

In the alternate 'silent synapse' model, glutamate signals produced by low-contrast stimuli (e.g. that fail to evoke starburst release) are 'unmatched' with GABA and ACh. In this model, unbalanced glutamate signals are rendered silent at DSGCs because they are processed predominantly by NMDA receptors (Figure 1D & E), which alone do not drive spiking (Sethuramanujam et al., 2016). NMDA receptors serve to amplify coincident ACh/GABA signals from starbursts that contain accurate directional information (Lee et al., 2010; Sethuramanujam et al., 2016). Thus, the requirement for high/low sensitivity bipolar cells to drive balanced E-I is obviated. Importantly, in this model, the bipolar inputs in the low-contrast regime are strictly modulatory and their strength is expected to alter response amplitude but not the direction tuning properties of DSGCs, contrasting with their role in the matched model.

The types of bipolar cells in the DS circuit have been described in great anatomical and physiological detail (Ding et al., 2016; Duan et al., 2014; Greene et al., 2016; Helmstaedter et al., 2013; Kim et al., 2014). Together these studies suggest that overlapping types of bipolar cells drive DSGCs and starbursts. However, these studies did not address whether individual bipolar cells provide common input to DSGCs and starbursts. Furthermore, previous anatomical studies relied on contact area analysis as a proxy for synaptic connectivity, which in some cases can be ambiguous (Ding et al., 2016). Therefore, whether starbursts and DSGCs are driven independently, or by shared input, remains an open question. Conclusive resolution of this issue would enable matched and silent synapse models for DS to be clearly distinguished.

At an operational level, both models ensure DS is maintained through the DSGC's dynamic range. However, one potentially important difference could manifest in the way NMDA receptors scale the DSGC's contrast response function. In the matched model, NMDA receptors scale the DSGC's response in a multiplicative manner, simply because they scale togther with non-NMDA receptor-mediated inputs (Murphy and Miller, 2003; Poleg-Polsky and Diamond, 2016a, b). Multiplicative scaling increases the gain of the DSGC input-output function (increase in R_{max}; Figure 1C). Conversely, in the silent synapse model, the NMDA/non-NMDA ratio changes with stimulus contrast (Figure 1E). Thus, NMDA receptors should amplify responses more strongly at low-contrasts and possibly increase the overall sensitivity of the DSGC's response to motion. A shift of the DSGC's input-output function along the contrast axis is considered an additive operation (Figure 1F) (Silver, 2010). This would be greatly advantageous, provided the strong amplification supplied by NMDA receptors does not disrupt DS coding in this regime.

To reconcile these conflicting views and further our understanding of the workings of the DS circuit, we monitored the sensitivity of NMDA and non-NMDA pathways simultaneously, in neighboring pairs of starbursts and DSGCs. This analysis indicated the presence of a high-sensitivity silent NMDA receptor-mediated pathway to DSGCs that was shared with starbursts (although starburst inputs were processed by AMPA receptors). Direct visualization of synapses with serial block-face EM (Denk and Horstmann, 2004), indicated an abundance of common input to DSGCs and starbursts from individual bipolar cells. Finally, pharmacological analysis of DSGC spiking responses recorded on a large-scale multi-electrode array indicated that NMDA receptors enhance the contrast sensitivity of

DSGC output while preserving their directional tuning properties, down to threshold contrast levels. Together, these findings lead us to propose a unifying 'silent synapse' model for DS, in which NMDA receptors help coordinate E/I in a way that maximizes output sensitivity (Figure 1F).

Results

In this study, our experiments address three specific questions. (1) What are the relative contrast sensitivities of NMDA vs. non-NMDA receptor mediated inputs to DSGCs? (2) Do starbursts and DSGCs share common bipolar cell input? (3) How do NMDA receptors modulate the DSGC's output as a function of stimulus direction vs. stimulus contrast?

A high-sensitivity glutamatergic pathway to DSGCs mediated by NMDA receptors

In whole-mount retinal preparations, genetically labeled starbursts and DSGCs were targeted for patch-clamp analysis using two-photon microscopy (Rivlin-Etzion et al., 2011; Trenholm et al., 2011). To accurately estimate the relative contrast sensitivities of NMDA and non-NMDA receptor-mediated inputs to DSGCs, we simultaneously measured responses to a series of moving spots of increasing contrasts (250 μm diameter, velocity ~ 1mm/s, Weber contrast 3-300%) in neighboring pairs of starbursts and DSGCs (Figure 2A). Peak synaptic responses were fit to the Naka-Rushton equation to estimate the contrast sensitivity of the input pathways (listed in Table S1). The starburst excitatory response (measured in whole-cell voltage-clamp mode, V_{HOLD} -60 mV) provided an internal control. This was particularly important because it helped overcome the alterations in the contrast response functions that arose from variability in the absolute sensitivity of individual cells estimated in different retinal preparations (Figure S1).

We found that excitatory inputs to starbursts were significantly more sensitive to stimulus contrast compared to both non-NMDA (nACh+AMPA) and GABA receptor-mediated inputs to DSGCs, measured at -60 mV (~E_{Cl}^-) and 0 mV (~$E_{Excitation}$), respectively (Figure 2B, C; $p < 0.05$). The non-NMDA and GABA inputs scaled almost perfectly together (Figure 2B, C; Table S1; $p = 0.41$). These measurements were consistent with the notion that bipolar cells with different sensitivities drive starbursts and DSGCs, and that E/I inputs to DSGCs scale together as a function of contrast (Poleg-Polsky and Diamond, 2016b). However, when inputs to DSGCs were measured at +40 mV, a more complex circuit arrangement was revealed.

At depolarized potentials, the sensitivity of synaptic inputs measured in DSGCs was well matched to that of starburst inputs (Figure 2B & D; Table S1; $p = 0.14$). The simplest interpretation of this finding is that depolarization reveals an additional contribution of NMDA receptors (by removing Mg^{2+} block) driven by a high-sensitivity pathway. Confirming this notion, the application of a selective NMDA receptor antagonist (50 μM D-AP5) shifted the DSGC's contrast response function to the right (Figure 2E; Table S1; $p < 0.05$). Similar results were obtained when NMDA and AMPA pathways were isolated pharmacologically (in the presence of $GABA_A$/ACh/kainate receptor antagonists; Figure 2F). However, the data under pharmacological isolation should be interpreted with caution,

as these conditions might exacerbate glutamate 'spillover' leading to an overestimate of NMDA receptor contributions (Sagdullaev et al., 2006; Zhang and Diamond, 2009).

Two lines of evidence suggest that the effects of AP5 are largely postsynaptic in origin. First, the sensitivity of the residual synaptic responses measured in D-AP5 was similar to the non-NMDA and inhibitory inputs measured in control conditions (compare Figure 2C and 2E; Table S1). Second, the NMDA antagonist did not affect the sensitivity of the starbursts (Figure S3) (Poleg-Polsky and Diamond, 2016a). Taken together, these results suggest that multiple bipolar cells with different sensitivities drive starbursts and DSGCs in parallel, but do so using distinct complements of glutamate receptors.

The relative high-sensitivity of the NMDA pathway to DSGCs was also apparent upon examining threshold responses. Responses to weak stimuli (< 20% Weber contrast) were detected in DSGCs only at the most depolarized potentials (+40 mV; Figure 2B), a signature of silent NMDA synapses (Kerchner and Nicoll, 2008). Indeed, these responses were completely blocked by D-AP5, confirming that they were mediated by NMDA receptors (Figure 2E; n = 5). In addition, the peak amplitude of the threshold responses evoked by preferred- and null-direction motion was similar (Figure S2; preferred = 132 ± 36 pA; null = 143 ± 45 pA; p = 0.41; responses measured at 12 ± 2 % Weber contrast). This not only suggests that glutamate release from bipolar cells is non-directional at its threshold (Park et al., 2014; Yonehara et al., 2013), but also confirmed that responses did not contain inhibitory currents, since inhibition measured at 0 mV was strongly DS at its threshold (note, threshold for inhibition was relatively higher compared with threshold for NMDA excitation; Figure S2). Importantly, the minimal contrast level for evoking NMDA inputs to DSGCs matched the threshold of inputs to starbursts (Figure 2B; *left* panel; Table S1). Together, these results support the notion that a high-sensitivity glutamate pathway drives DSGCs and starbursts in parallel, and establishes NMDA as the dominant synaptic conductance in DSGCs near threshold contrasts.

Previous studies provided mixed views on whether presynaptic pathways to DSGCs, including those mediated by AMPA and NMDA receptors, scale proportionately as a function of contrast (Lipin et al., 2015; Poleg-Polsky and Diamond, 2016b; Sethuramanujam et al., 2016; Stafford et al., 2014). Here, the paired recordings directly demonstrate that high-sensitive inputs to starbursts scale with NMDA receptor mediated inputs, but not with GABA/AMPA/ACh inputs to DSGCs (Figure 2). These differences were not easily apparent if DSGC responses alone were averaged over a small population without accounting for the contrast sensitivity of a nearby starburst (Figure S1). This is likely one source for the inconsistencies in previous studies. It is also possible that different experimental conditions contribute to some of the observed differences.

A shared glutamatergic pathway to starbursts and DSGCs

The finding that glutamate receptor-mediated synaptic responses in starbursts and DSGCs could share the same sensitivity and threshold suggests that they arise either from the same presynaptic bipolar cells, or from different bipolar cells with similar sensitivities. To examine the functional connectivity patterns, we next examined the degree to which spontaneous NMDA and AMPA receptor-mediated inputs were temporally correlated in

neighboring starbursts and DSGCs with overlapping dendritic fields (inter-somatic distance < 50 μm; Figure 3). In these experiments, AMPA and NMDA receptor-mediated activity was isolated pharmacologically using the cocktail of GABAA/nACh/kainate receptor antagonists. The presence of the kainate receptor antagonist (10μM UBP310) which selectively hyperpolarizes OFF bipolar cells (Borghuis et al., 2014), was used to limit activity from the OFF pathway. Under these conditions, spontaneous EPSCs occurred in bursts of varying amplitudes (10-300 pA) that could last for hundreds of milliseconds (Figure 3A & D), reflecting the coordinated release of multiple vesicles and possibly glutamate 'spill-over' (Sagdullaev et al., 2006; Zhang and Diamond, 2009). While this made it difficult to carry out a quantitative analysis to estimate the precise number of shared inputs to starbursts and DSGCs (Grimes et al., 2014), it provided a strong indication of the pharmacological properties of shared and unshared input occurring on a coarser scale, as described below.

Spontaneous activity in starbursts and DSGCs was strongly correlated (CC = 0.57 ± 0.08; n = 6) on a millisecond time-scale with a half-width at half-maximum of 70 ± 11 ms (Figure 3C). This strong and temporally precise correlation observed between starburst and DSGC inputs indicates a common presynaptic source (Grimes et al., 2014; Trong and Rieke, 2008). Application of D-AP5 strongly reduced correlated activity (Figure 3B, C; CC = 0.19 ± 0.08; n = 6; $p < 0.001$). Similar results were obtained when NMDA receptors were blocked postsynaptically by either measuring AMPA EPSCs at -60 mV ($CC_{-60\ mV} = 0.16 \pm 0.03$; n = 3; data not shown); or by including MK-801 in the electrode solution (Figure 3D-F; $CC_{initial} = 0.6 \pm 0.09$; $CC_{late} = 0.2 \pm 0.04$; n = 6; $p < 0.01$). Together, these results indicate that the effect of blocking NMDA on correlated activity was largely postsynaptic in origin. It is important to note that the weak correlations observed during NMDA receptor blockade is not a result of reducing the amplitude of spontaneous events in DSGCs. The example DSGCs shown in Figure 3 were chosen to illustrate this point. In these DSGCs, the extent by which NMDA blockade reduced responses were different (~70% Figure 3A,B vs. ~25% reduction Figure 3D,E), yet the residual non-NMDA events were correlated with starburst activity to a similar extent (Figure 3C, F). In addition, the weak correlations in the AMPA receptor-mediated inputs, in conjunction with the distinct contrast sensitivities of AMPA and NMDA inputs (Figure 2F) argue against the idea that inhibitory receptor blockade induced widespread synchrony. These observations suggest that AMPA receptor driven synapses in DSGCs are not shared with starbursts to the same extent as NMDA receptor driven synapses. While it is not possible to directly determine whether spontaneous correlated activity derives from the high- or low sensitivity glutamate pathway in the DS circuit, the finding that NMDA receptors alone mediate the threshold response in DSGCs (Figure 2B) leads us to posit that it is the high sensitivity pathway that is shared.

Anatomical evidence for common synaptic input to starbursts and DSCGs

While previous studies have identified overlapping types of bipolar cells driving starbursts and DSGCs, whether an individual bipolar cell can contact both a starburst and a DSGC is not clear (Ding et al., 2016; Duan et al., 2014; Greene et al., 2016; Helmstaedter et al., 2013; Kim et al., 2014). To determine whether the underlying anatomical connectivity supports the functional evidence for common input, we next examined connectivity in a serial block-face

EM dataset in which intracellular structures were preserved (Ding et al., 2016). Bipolar cell ribbon synapses could be identified by the ribbon-containing terminal apposed to two post-synaptic structures in the form of a dyad (Figure 4A, B). The ribbons themselves could be unequivocally identified in 3D as faint gray sheets decorated by a halo of vesicles (Ding et al., 2016), rather than as intense electron dense structures that are typically observed in post-stained serial sections (Figure 4A, B).

To investigate the possibility of common input, we reconstructed an entire axonal terminal of a BC contacting the ON dendrites of a DSGC. In this case, the bipolar cell was identified as type BC5t based on its characteristic 'thick' stratification pattern (Ding et al., 2016; Greene et al., 2016). In this terminal, we identified 22 ribbon synapses distributed across the axonal tree (Figure 4C). To determine which cells this bipolar cell activated, we partially reconstructed the two postsynaptic cells contacted by each of the identified ribbon synapses. This analysis revealed that BC5t contacted starbursts, DSGCs as well as non-starburst amacrine cells (wide- and narrow-field amacrine cells; Figure 4D). Of the 9 synapses made with DSGCs, 4 were shared with starbursts, 3 with other DSGCs and 2 with wide-field amacrine cells.

Rather than repeating the similar analysis for many bipolar cells, which is a significant undertaking, we took a complementary approach to confirm the prevalence of common input to DSGCs and starbursts. This entailed viewing shared connections from the perspective of the DSGC. We annotated 64 ribbon synapses (arising from ~20-30 bipolar cells, assuming each bipolar cell makes on average 2-3 synapses/DSGC, as they do for starbursts) (Ding et al., 2016), contacting a single DSGC in the ON sublamina of the inner-plexiform layer and then traced the second post-synaptic partner present in the dyad (Figure 4E). This analysis revealed that dyads in a DSGC were shared with another DSGC (53%), with an ON starburst (41%; Figure 4E & F), or in the rare case with a wide-field amacrine cell (6%). While these analyses preclude the identification of the types of bipolar cells contacting starbursts and DSGCs, they strongly indicate that these cells share bipolar cell input, both on the fine spatial scale of dyads (Dacheux et al., 2003), as well as on the coarser scale of whole bipolar cell axon terminals, providing strong support for our physiological measurements indicating common input.

'Arithmetical' scaling operations mediated by NMDA receptors

Having gained functional and anatomical evidence for the silent synapse model we next sought to understand the rationale for such a design. We envisioned that the high sensitivity pathway would have the largest impact on responses evoked by low-contrast stimuli, but how it affected the DSGC's input-output function (response gain and/or C_{50}) and DS coding at lower contrasts was harder to predict based on the conductance measurements alone. We employed a simple two-compartmental computational model (Figure 5; see Supplemental Methods for details) to build an intuition of how NMDA receptors may behave differently across stimulus contrasts and directions. Responses were driven by inhibitory and excitatory synaptic inputs that grew in contrast, similar to our experimental measurements. To simulate stimulus direction, excitation was set to be non-directional while GABA inhibition was highly directional (Poleg-Polsky and Diamond, 2016a). Interestingly, although the DSGCs

spiking response was modulated by stimulus contrast and stimulus direction to a similar extent, NMDA receptors had a different effect in each context (Figures 5).

In the matched model configuration, where synaptic inputs scale proportionately as a function of contrast, we found that NMDA-mediated inputs amplified responses in a multiplicative manner (Murphy and Miller, 2003; Poleg-Polsky and Diamond, 2016a). This is indicated by the stable fractional contribution of NMDA receptors across the entire contrast range (Figure 5A, *right axis*). However, in a similar model in which the contrast sensitivity of the NMDA inputs was increased according to our experimental measurements (Figure 2C-E), the NMDA receptor contribution to the DSGC's spiking response became highly dependent on stimulus contrast (Figure 5D, *right axis*), being maximal at the lowest contrasts. As a result, the contrast response function in the absence of NMDA receptors was rightward shifted (C_{50}: 26.5% Weber contrast in control; 32.5% without NMDA receptors) (Figure 5D). However, as this increase in sensitivity was an effect of a disproportionate contrast-dependent scaling of the DSGC's spiking response amplitude (y–scaling), this operation can be considered ‘pseudo-additive’, to distinguish it from real x–scaling operations (Silver, 2010). Interestingly, even at low-contrasts (30%) where NMDA receptors strongly amplify responses, NMDA receptors scaled responses in a way that preserved DS tuning properties of the model DSGC (Figure 5G), similar to their effects observed at higher contrasts (Poleg-Polsky and Diamond, 2016a). Thus, a simple model that captures the multiplicative effects of NMDA receptors, predicts that the high-sensitivity NMDA pathway produces an additive scaling of the DSGCs output as a function of contrast.

To understand the synaptic mechanisms underlying the context-dependent modulation by NMDA receptors we examined the synaptic currents/conductances underlying the DSGC's responses under different conditions (Figure 5B, E & H). In the case of the silent synapse model, at low-contrasts, the total current through the NMDA receptors was large relative to the non-NMDA and GABA receptor-mediated current (Figure 5E). The NMDA/non-NMDA ratio subsequently falls with increasing contrast because the non-NMDA conductance sharply increases (Figure 5F). This occurs despite the voltage-dependent increase of the absolute NMDA conductance observed with increasing contrasts. Consequently, the relative contribution of NMDA to spiking decreases over the contrast range, resulting in the pseudo-additive scaling operation observed in the silent synapse model (Figure 5D). However, in other cases (direction tuning or in the matched model), the NMDA/non-NMDA conductance ratio *increases* with response magnitude (Figure 5C & I), giving rise to multiplicative scaling (Figure 5A & G). Note, if NMDA receptors were made to be voltage-independent in the model, the multiplicative scaling properties on the directional responses are lost (Figure S4) (Poleg-Polsky and Diamond, 2016a). Thus, these simple models simulating the DSGC's responses over direction and contrast indicate that the relative NMDA conductance (rather than absolute NMDA conductance/current) is a key factor that determines how NMDA receptors shape responses.

To test these model predictions, we examined the effects of blocking NMDA receptors on the spiking behavior of DSGCs. A multi-electrode array (MEA) was used to record activity from a population of DSGCs across a range of directions and contrast levels (8 directions; 5-300% Weber contrast). ON-OFF DSGCs were distinguished from other ganglion cells

based on their direction and speed tuning (Figure 6A; Figure S5; see Methods). A heat map of the average number of spikes/trial measured across the population of DSGCs plotted as a function of direction and contrast (Figure 6C), depicts for the first time the ability of mouse DSGCs to maintain their directional tuning properties across a large contrast range, consistent with the behavior of their counterparts in the rabbit retina (Grzywacz and Amthor, 2007; Nowak et al., 2011). However, small but statistically significant contrast-dependent changes in tuning reflected in direction selectivity index (DSI; see methods) were observed in the low ($DSI_{10\%}$ = 0.46 ± 0.04; $DSI_{20\%}$ = 0.61 ± 0.02; $p < 0.005$, Wilcoxon signed-rank test) and high-contrast ranges ($DSI_{150\%}$ = 0.57 ± 0.02; $DSI_{300\%}$ = 0.47 ± 0.02; $p < 0.05$, Wilcoxon signed-rank test).

We found blocking NMDA receptors with D-AP5 reversibly reduced the response amplitude for all four populations of ON-OFF DSGCs (Figure 6B) and thus the data from all types were combined. Consistent with previous studies, the NMDA receptor antagonist did not strongly affect the directional tuning properties of DSGCs (Control $DSI_{40\%}$ = 0.65 ± 0.01; D-AP5 $DSI_{40\%}$ = 0.63 ± 0.02; $p = 0.39$; Wilcoxon signed-rank test; Figure 6C-E). Moreover, the fractional response blocked by NMDA antagonists did not change with direction across a range of stimulus contrasts (Figure 6G & H), indicating the robustness of the multiplicative scaling properties of NMDA receptors (Poleg-Polsky and Diamond, 2016a).

However, when viewed as a function of stimulus contrast, we found NMDA receptors did not scale responses in a multiplicative manner, consistent with the prediction of our silent synapse model neuron. D-AP5 reduced responses evoked by low-contrast stimuli (< 20% contrast) more strongly than it reduced responses to high-contrast stimuli (> 20% contrast; Figure 6F & H; $p < 0.001$, Wilcoxon signed-rank test). This resulted in an increase in both the semi-saturation constant (control: 55.5 ± 5% Weber contrast; AP5: 72.6 ± 4%; $p < 0.0001$, Wilcoxon signed-rank test) and the absolute threshold (control: 30 ± 3%; AP5: 51 ± 5%; $p < 0.0001$; Wilcoxon signed-rank test) of the DSGC's contrast response function, which are hallmarks of additive operations (Figure 6F) (Silver, 2010). The NMDA transformation across the majority of the contrast range is explained by arithmetically scaling the responses to increasing contrasts in the y-dimension, using additive (77%) and multiplicative (23%) scaling factors (See Figure S6). Importantly, the additive shifts occurred for all stimulus directions, as indicated by the % block plots (Figure 6G & H). In contrast, simultaneously recorded ON ganglion cells with brisk transient responses exhibited only a minor change in their contrast sensitivity upon D-AP5 application (C50 in control: 27.1 ± 1%; C_{50} in AP5: 30.0 ± 1%; $p < 0.0001$, Wilcoxon signed-rank test; Figure S5), indicating that time-dependent changes in overall retinal sensitivity did not confound the pharmacology. Thus, NMDA receptors instantiate multiple ‘arithmetical’ operations that enhance the DSGC's sensitivity, without compromising direction encoding.

Importantly, the large contribution of NMDA receptors to the low-contrast response is not due to a simple thresholding effect. This is directly indicated by the finding that responses of similar amplitudes to stimuli moving in non-preferred directions (high-contrast) were significantly less affected by D-AP5 (Figure 6H). This can be seen more clearly, when the % block is plotted against the number of spikes (Figure S6C). The reason for the different amounts of blocks under these two conditions (low-contrast in the preferred direction and

high-contrast in the null direction) is that at low-contrasts, the NMDA synaptic conductance is the dominant conductance (Figure 2B); while in the non-preferred directions, it is dwarfed by the opposing inhibitory conductances that combine to generate weak spiking responses (Taylor and Vaney, 2002). Therefore, the contribution of NMDA receptors in this context depends on their conductance relative to other synaptic conductances. Thus, the large contribution of NMDA receptors at low-contrasts, imparted by the high-sensitive pathway (Figure 5E), is paramount to creating the observed pseudo-additive effect of NMDA on contrast-modulated DSGC spiking responses.

Discussion

Our results characterizing the input/output function of DSGCs and starburst amacrine cells shed new light on the precise arrangement of the feedforward circuitry, highlighting the computational advantages gained by the differential expression of AMPA/NMDA receptors at specific inner retinal synapses.

A unified model for contrast invariant DS tuning utilizing silent synapses

Whether starbursts and DSGCs receive common input from bipolar cells is an important aspect of the DS circuit that remains debated (Poleg-Polsky and Diamond, 2016b; Helmstaedter et al., 2013). Here, we unequivocally identify a high degree of shared input to starbursts and DSGCs in a recent SBEM dataset (Ding et al., 2016). These results effectively complement previous studies that identify the types of bipolar cells driving starbursts and DSGCs, and together suggest that the most likely candidates for common input are the bipolar cell types 5i, 5o and 5t (BC5s) (Ding et al., 2016; Duan et al., 2014; Greene et al., 2016; Helmstaedter et al., 2013; Kim et al., 2014; Seung personal communication). In addition, the likely sources of uncommon input are the type 7 bipolar cells, which make strong contact with starbursts (20-45%; Helmstaedter et al., 2013; Greene et al., 2016; Ding et al., 2016) but not DSGCs; and an anomalous source of glutamate from a specialized subset of VGlut3^{+} amacrine cells, which appear to drive DSGCs but not to starbursts (Lee et al., 2014).

The presence of profuse shared afferents reinforces the general question of how feed-forward E/I can be balanced in the face of threshold circuit non-linearities. Other feedforward circuits appear to circumvent non-linear processing using several specializations, all which lead to the preferential recruitment of inhibitory interneurons. For example, afferent inputs/projections to inhibitory neurons may have higher vesicular release probabilities (Acsady et al., 1998; Maccaferri et al., 1998; Toth et al., 2000), a larger number of synapses (Bruno and Simons, 2002; Stokes and Isaacson, 2010), and/or AMPA receptor subtypes with larger unitary conductances relative to synapses driving principal neurons (Cruikshank et al., 2007; Gabernet et al., 2005; Lawrence and McBain, 2003). At thalamocortical synapses, the AMPA/NMDA receptor ratio differs between principal cells and interneurons, in a way that drives inhibition with higher fidelity (Angulo et al., 1999; Hull et al., 2009; Krukowski and Miller, 2001). However, the drawback of driving inhibitory pathways more effectively is that it decreases the overall sensitivity of the circuit (Poleg-Polsky and Diamond, 2016b).

Here we propose a novel scheme in which silent NMDA receptors play a dominant role in orchestrating E-I balance at low contrast, while maximizing circuit sensitivity (Figure 1D-F). The rationale for NMDA receptor expression becomes clear when considered in relation with the starburst input/output. Starbursts only release their neurotransmitters when their inputs are stimulated to 38 ± 5% of their maximum (Figure 2C). Because DSGCs are driven by shared input, in this regime, presynaptic glutamate and GABA signals are not balanced. As these glutamate signals are non-directional (Figure S2) (Park et al., 2014; Yonehara et al., 2013), they would likely produce non-directional spiking responses in DSGCs if conventional AMPA synapses were utilized. By using silent synapses, DSGC responses become reliant on coincident starburst cholinergic inputs for their activation (Brombas et al., 2017; Sethuramanujam et al., 2016), and thus circumvent the potential deleterious effects of non-linear processing by starbursts.

We further propose that the high sensitive silent NMDA receptor mediated inputs to DSGCs and the AMPA/KA receptor mediated inputs to starburst cells originate from the same bipolar presynaptic terminals. This is based on the findings that: 1) ~ 40% of the dyadic input to DSGCs are shared with starbursts (Figure 4). 2) NMDA inputs to DSGCs and AMPA inputs to starburst have similar threshold sensitivities (Figure 2); and 3) spontaneous NMDA but not AMPA receptor mediated activity in DSGCs was strongly correlated with starburst input (Figure 3). It should be mentioned that the measurements of correlated activity were performed under artificial conditions to isolate AMPA and NMDA receptor components, which could exaggerate correlations through indirect network mechanisms. For example, NMDA receptors that have a higher affinity for glutamate compared to AMPA receptors could in theory sense glutamate ‘spillover’ from synapses that drive starbursts, especially under conditions in which GABA receptors are blocked (Sagdullaev et al., 2006; Zhang and Diamond, 2009). However, we found spontaneous NMDA receptor-mediated EPSCs in DSGCs to be almost as large as AMPA EPSCs measured in starbursts making it unlikely that NMDA inputs were mediated solely by spillover mechanisms, which tend to drive relatively weaker responses in other areas of the brain (Szapiro and Barbour, 2007). Nevertheless, future studies using immuno-EM are required to confirm that AMPA and NMDA receptors are differentially expressed postsynaptically at the level of single bipolar dyads. The age-old ‘rule’ stating that only one of the two post-synaptic processes at a dyad expresses a given ionotropic glutamate receptor subtype (Boycott and Wassle, 1999), suggests this as an intriguing possibility.

In addition to silent synapses, four other important circuit features ensure that DSGCs are able to encode direction under low-contrast conditions. First, GABAergic inhibition to DSGCs was found to be DS at the lowest detectable contrast (Figure S2). This is consistent with the idea that starburst dendrites strongly rely on high-threshold voltage-gated Ca^{2+} channels for transmitter release as well as for generating robust directional responses (Hausselt et al., 2007; Tukker et al., 2004). Second, in contrast to earlier reports (Lee et al., 2010), we found GABA and ACh inputs to be activated at similar contrast thresholds (Figure 2C). The precise activation of cholinergic inputs could be inferred from measurements of excitation made at -60 mV, because they are known to dominate the non-NMDA excitatory inputs to DSGCs at low stimulus contrasts (Sethuramanujam et al., 2016). Although cholinergic signals are non-DS, the combination of E/I signals generated by the starburst

network contain accurate direction information (Sethuramanujam et al., 2016). Third, even near contrast threshold, where NMDA conductances are large (1 nS G_{max} estimated at +40 mV), ACh input never 'kicks' NMDA receptors into a self-regenerating mode. This indicates that NMDA receptor activity is well balanced by opposing conductances, likely provided by the combination of GABA (Krukowski and Miller, 2001; Poleg-Polsky and Diamond, 2016a; Rivadulla et al., 2001), voltage-dependent K^+ and leak conductances (Ferster and Miller, 2000; London and Hausser, 2005; Schiller et al., 2000). Together, this ensures that NMDA receptors amplify starburst ACh/GABA signals without altering the direction coding of DSGCs. Fourth, the neighboring DSGCs receive common input from bipolar cells (~ 50% dyadic connections are shared with other DSGCs; Figure 4), regardless of the direction they code. This suggests that NMDA modulation would occur in a correlated way across the four types of DSGCs, helping to preserve the population code (Zylberberg et al., 2016). Thus, it appears that silent synapses engage with diverse mechanisms to produce a robust DS code, down to threshold levels.

In one respect, the silent synapse model appears inefficient compared to the matched model, as scaling glutamate and ACh in proportion would avoid the 'silent' regime where glutamate does not produce spiking responses. However, if ACh and NMDA inputs had similar contrast scaling, then their interactions at threshold contrasts would be weak (Figure 5), as there would only be a few glutamate-bound NMDA receptors. By sharing signals generated by the high-sensitivity pathway, many NMDA synapses are 'primed' to amplify even weak coincident cholinergic inputs, requiring fewer starburst inputs to generate a spiking response. The shifting of the DSGC's input-output function along the contrast axis by NMDA receptors highlights the functional advantage of the silent synapse over the matched model, where responses are expected to scale purely multiplicatively. By sharing starburst input with DSGCs, the DS circuit ensures that information carried by high-sensitive bipolar cells is fully utilized.

Contact for Reagent and Resource Sharing

Further information and requests for resources and reagents should be directed to and will be fulfilled by the Lead Contact, Dr. Gautam B. Awatramani (gautam@uvic.ca).

Experimental Model and Subject Details

Animals

Experiments were performed using healthy adult (either sex) C57Bl6 (RRID: IMSR_JAX: 000664), $Hb9^{eGFP}$ (RRID: MGI_109160), TRHR-GFP (RRID:MMRRC_030036-UCD) and $Chat^{cre}$ (RRID: MGI_5475195) crossed with reporter mice, Ai9 (RRID: MGI_3809523). Animals were housed in 12hr light-dark cycles, in groups up to 5 animals per cage. All procedures were performed in accordance with the Canadian Council on Animal Care and approved by the University of Victoria's Animal Care Committee or Duke University's Animal Care and Use Committee.

Method Details

Dual Patch Clamp Recordings

Mice were dark-adapted for approximately 30–60 min before being briefly anesthetized and decapitated. The retina was dissected in Ringer's solution under infrared light. The isolated retina was then mounted on a 0.22 mm membrane filter (Millipore) with a pre-cut window to allow light to reach the retina and enabling the preparation to be viewed with infrared light using a Spot RT3 CCD camera (Diagnostic Instruments) attached to an upright Olympus BX51 WI fluorescent microscope outfitted with a 40× water-immersion lens (Olympus Canada). The isolated retina was then perfused with warmed Ringer's solution (35–37 °C) containing 110 mM NaCl, 2.5 mM KCl, 1 mM $CaCl_2$, 1. 6 mM $MgCl_2$, 10 mM dextrose and 22 mM $NaHCO_3$ that was bubbled with carbogen (95% O_2:5% CO_2).Unless otherwise noted, all reagents were purchased from Sigma-Aldrich Canada. NBQX, D-AP5, MK-801 and UBP310 were purchased from ABCAM Biochemicals.

DSGCs and starbursts were identified using two-photon laser-scanning microscopy techniques. Voltage-clamp whole-cell recordings were made using 4–7-MΩ electrodes containing 112. 5 mM $CH_3C_sO_3S$, 7.75 mM CsCl, 1 mM $MgSO_4$, 10 mM EGTA, 10 mM HEPES, 5 mM QX-314-bromide (Tocris) and 100 μM spermine (ABCAM Biochemicals). The pH was adjusted to 7. 4 with CsOH. The reversal potential for chloride was calculated to be -56 mV. The recordings were neither corrected for series resistance nor the junction potential. Recordings were made with a MultiClamp 700B amplifier (Molecular Devices). Signals were digitized at 10 kHz (PCI-6036E acquisition board, National Instruments) and acquired using custom software written in LabVIEW. The traces were viewed and analyzed offline with custom written software in MATLAB.

Visual stimuli were produced using a digital light projector (Hitachi Cpx1, refresh rate 75 Hz), focused onto the outer segments of the photoreceptors using the sub-stage condenser. The background luminance, measured with a calibrated spectrophotometer (Ocean Optics), was set to 10 photoisomerisations/s (R*/sec). Stimuli were created in the Matlab environment (Psychtoolbox). Spots (250 μm diameter) with positive contrasts, ranging between 3% and 300% (Weber contrast) were moved across the retina at a velocity of 1mm/s, along the preferred or null axis of the DSGC, as indicated. The responses were fitted to the Naka Rushton equation R_{max} (C^n /(C^n +$C_{50}{}^n$)), where C indicates the contrast, R_{max} is the maximum response, C50 the semi-saturation constant and n is a coefficient proportional to the slope of the contrast response function at C50. Correlated activity in starbursts and DSGCs were estimated by comparing the spontaneous activity in dark over 5 second intervals.

Multi-Electrode Array Recordings

Dorsal peripheral retina was dissected and mounted with ganglion cell side down on an array of 519 electrodes with 30 μm spacing, covering a hexagonal region of ~0.5 μm (Yu et al., 2017). The retina was perfused with Ames' solution (30-31°C, 7-12 mL/min) bubbled with 95% O_2 and 5% CO_2, pH 7.4. Recordings were analyzed offline to identify and sort the spikes of different cells, as described previously (Field et al., 2007). Visual stimuli were

presented on an OLED video display (emagin) using custom software written in MATLAB (Mathworks); stimuli were focused onto the photoreceptor layer. Light intensities were set using a calibrated photodiode (Gamma Scientific). Experiments were performed at a light intensity corresponding to ~7000 P*/cone/s (for the middle wavelength sensitive opsin).

Candidate spike events were detected using a threshold on each electrode, and voltage waveforms on the electrode and nearby electrodes around the time of the spike were extracted. Clusters of similar spike waveforms were identified as candidate neurons if they exhibited a refractory period and accounted for more than 100 spikes in recording over 30 min. Duplicate spike trains identified across different electrodes were identified by temporal cross-correlation and removed. DSGCs were identified from the magnitudes of vector summed response to square-wave drifting gratings moving in 8 directions (spatial and temporal periods 960 μm and 2 seconds, respectively), using a Gaussian Mixture model (Figure S5C). The cluster with larger average magnitudes identified DSGCs. ON and ON-OFF DSGCs were further segregated by their speed tuning. Square-wave gratings drifting at 8 speeds (ranging from 0.04 to 4.8 mm/s) were used to measure speed tuning curves (data not shown). Cells with broad speed tuning were identified as ON-OFF DSGCs, while cells that preferred lower speeds were identified as ON DSGCs. ON-OFF DSGCs exhibited 4 direction preferences while ON DSGCs exhibited 3 (data now shown). The relative direction preference was determined by using the electrophysiological image (EI), which is a movie of the average electrical activity produced across the electrode array by a neuron. Since axons of dorsal RGCs travel ventral, DSGCs with preferred direction matching the axon direction were identified as superior DSGCs, other directions were determined by whether the retina was dissected from the left or right eye. Direction tuning curves and contrast response functions (Figure 6) were measured with moving bar stimuli. The bar was 240 μm wide on the retina and moved at 960 μm/s. The direction-tuning curve was centered at the preferred direction and fit with a cosine or Gaussian equation, as indicated (Nowak et al., 2011).

Electron Microscopy Analysis

A previously published data set acquired using scanning SBEM was analyzed (retina k0563; Ding et al., 2016). Voxel dimensions were 12 × 12 × 25 nanometer (nm) (x, y, and z, respectively). Potential DSGCs were first identified as ganglion cells with bistratified morphology in the IPL. Next, synapses from starbursts on the dendrites of these cells were identified; partial reconstruction of the ON and OFF starbursts confirmed their co-stratification with the ganglion cell dendrites indicating a DSGC. Bipolar cell ribbon synapses on the DSGC dendrites were identified and other post-synaptic elements were annotated by partial dendritic reconstruction (Figure 4). The whole axon terminal of a bipolar cell synapsing with the DSGC was reconstructed to annotate its ribbon synapses and identify dyadic partners. All analyses were performed by tracing skeletons and annotating synapses using the Knossos software package (www.knossostool.org). Volumetric reconstructions of synapses were performed using ITK-SNAP (www.itksnap.org) (Yushkevich et al., 2006).

Simulations

A simple two-compartment model containing a thin passive compartment attached to an active soma was built in the NEURON simulation environment (Hines and Carnevale, 1997). The synaptic inputs (NMD A, non-NMDA and inhibition) were placed at the end of the thin passive compartment. Physical parameters were set such that electrotonic properties of the model neuron allowed the membrane voltage at the synaptic site to vary from that of the soma (See Table M1 below). The synaptic inputs were modelled with reversal potentials for non-NMDA and NMDA at 0mV and inhibition at -60mV Inhibitory and non-NMDA conductances were implemented with the built-in Exp2Syn point process of the NEURON environment, and NMDA was implemented by modifying the Exp2Syn process to include a voltage function [$g(v) = G_{max} / (1 + 0.213 * e^{-gamma*v})$; n = 0.25, gamma = 0.08]. To simulate voltage independent NMDA activity, g was set to 20% of G_{max} (the conductance at -30mV, using the equation above), at all voltages.

Contrast responses were simulated by scaling the synaptic input conductances to the Naka-Rushton fits (Table M2; Figure 2). Note that these values were slightly different from Table S1 as they are taken by fitting the average responses. For the ‘matched’ models, the NMDA conductances were scaled to the non-NMDA Naka-Rushton fit. For direction, the amplitude of non-NMDA and NMDA conductances were set as constant, while the amplitude and timing of inhibitory conductances were varied simulating 16 different directions (11.25° apart). These values were modulated such that the model output best approximated the directional tuning observed in the MEA experiments.

In the spiking models, the soma was built with active properties (Nav, Kv, noise) implemented using a stochastic Hodgkin-Huxley (HHst) model (Linaro et al., 2011). Spike outputs were simulated over 20 trials with unique pseudo-random noise provided by HHst. The total number of spikes generated by the synaptic inputs was estimated as the response.

Quantification and Statistical Analysis

All population data has been expressed as mean ± SEM and are indicated, along with the number of samples, in the figure legend. Student's t test or a Wilcoxon signed-rank test was used to compare values under different conditions (unless indicated in the main text, Student's t test was used), and the differences were considered significant when $p \leq 0.05$.

Data and Software Availability

The data analysis is available on request from the Lead Contact.

Supplementary Material

Refer to Web version on PubMed Central for supplementary material.

Acknowledgments

We thank Drs. Jeff Diamond, Alon Poleg-Polsky, Jon Cafaro, Court Hull, Kerry Delaney and Ben Murphy-Baum for their useful discussions and comments on the manuscript. J. Boyd (University of British Columbia) for help with two-photon imaging software, A. Sher, J. Leung and Laura Hanson for providing helpful technical support.

This work was supported by operating grants from the NIH/NEI EY024567 (G.D.F), Foundation Fighting Blindness (Canada) and Canadian Institutes for Health Research (CIHR- 130268-2013) awarded to G.B.A.

References

Acsady L, Kamondi A, Sik A, Freund T, Buzsaki G. GABAergic cells are the major postsynaptic targets of mossy fibers in the rat hippocampus. J Neurosci. 1998; 18:3386–3403. [PubMed: 9547246]

Angulo MC, Rossier J, Audinat E. Postsynaptic glutamate receptors and integrative properties of fast-spiking interneurons in the rat neocortex. J Neurophysiol. 1999; 82:1295–1302. [PubMed: 10482748]

Borghuis BG, Looger LL, Tomita S, Demb JB. Kainate receptors mediate signaling in both transient and sustained OFF bipolar cell pathways in mouse retina. J Neurosci. 2014; 34:6128–6139. [PubMed: 24790183]

Boycott B, Wassle H. Parallel processing in the mammalian retina: the Proctor Lecture. Invest Ophthalmol Vis Sci. 1999; 40:1313–1327. [PubMed: 10359312]

Brombas A, Kalita-de Croft S, Cooper-Williams EJ, Williams SR. Dendro-dendritic cholinergic excitation controls dendritic spike initiation in retinal ganglion cells. Nat Commun. 2017; 8:15683. [PubMed: 28589928]

Bruno RM, Simons DJ. Feedforward mechanisms of excitatory and inhibitory cortical receptive fields. J Neurosci. 2002; 22:10966–10975. [PubMed: 12486192]

Buldyrev I, Puthussery T, Taylor WR. Synaptic pathways that shape the excitatory drive in an OFF retinal ganglion cell. J Neurophysiol. 2012; 107:1795–1807. [PubMed: 22205648]

Cruikshank SJ, Lewis TJ, Connors BW. Synaptic basis for intense thalamocortical activation of feedforward inhibitory cells in neocortex. Nat Neurosci. 2007; 10:462–468. [PubMed: 17334362]

Dacheux RF, Chimento MF, Amthor FR. Synaptic input to the on-off directionally selective ganglion cell in the rabbit retina. J Comp Neurol. 2003; 456:267–278. [PubMed: 12528191]

Denk W, Horstmann H. Serial block-face scanning electron microscopy to reconstruct three-dimensional tissue nanostructure. PLoS Biol. 2004; 2:e329. [PubMed: 15514700]

Diamond JS, Copenhagen DR. The relationship between light-evoked synaptic excitation and spiking behaviour of salamander retinal ganglion cells. J Physiol. 1995; 487(Pt 3):711–725. [PubMed: 8544133]

Ding H, Smith RG, Poleg-Polsky A, Diamond JS, Briggman KL. Species-specific wiring for direction selectivity in the mammalian retina. Nature. 2016; 535:105–110. [PubMed: 27350241]

Duan X, Krishnaswamy A, De la Huerta I, Sanes JR. Type II cadherins guide assembly of a direction-selective retinal circuit. Cell. 2014; 158:793–807. [PubMed: 25126785]

Ferster D, Miller KD. Neural mechanisms of orientation selectivity in the visual cortex. Annu Rev Neurosci. 2000; 23:441–471. [PubMed: 10845071]

Field GD, Sher A, Gauthier JL, Greschner M, Shlens J, Litke AM, Chichilnisky EJ. Spatial properties and functional organization of small bistratified ganglion cells in primate retina. J Neurosci. 2007; 27:13261–13272. [PubMed: 18045920]

Gabernet L, Jadhav SP, Feldman DE, Carandini M, Scanziani M. Somatosensory integration controlled by dynamic thalamocortical feed-forward inhibition. Neuron. 2005; 48:315–327. [PubMed: 16242411]

Greene MJ, Kim JS, Seung HS. EyeWirers. Analogous Convergence of Sustained and Transient Inputs in Parallel On and Off Pathways for Retinal Motion Computation. Cell Rep. 2016; 14:1892–1900. [PubMed: 26904938]

Grimes WN, Hoon M, Briggman KL, Wong RO, Rieke F. Cross-synaptic synchrony and transmission of signal and noise across the mouse retina. Elife. 2014; 3:e03892. [PubMed: 25180102]

Grzywacz NM, Amthor FR. Robust directional computation in on-off directionally selective ganglion cells of rabbit retina. Vis Neurosci. 2007; 24:647–661. [PubMed: 17900380]

Hanse E, Seth H, Riebe I. AMPA-silent synapses in brain development and pathology. Nat Rev Neurosci. 2013; 14:839–850. [PubMed: 24201185]

Hausselt SE, Euler T, Detwiler PB, Denk W. A dendrite-autonomous mechanism for direction selectivity in retinal starburst amacrine cells. PLoS Biol. 2007; 5:e185. [PubMed: 17622194]

Helmstaedter M, Briggman KL, Turaga SC, Jain V, Seung HS, Denk W. Connectomic reconstruction of the inner plexiform layer in the mouse retina. Nature. 2013; 500:168–174. [PubMed: 23925239]

Herrero JL, Gieselmann MA, Sanayei M, Thiele A. Attention-induced variance and noise correlation reduction in macaque V1 is mediated by NMDA receptors. Neuron. 2013; 78:729–739. [PubMed: 23719166]

Hines ML, Carnevale NT. The NEURON simulation environment. Neural Comput. 1997; 9:1179–1209. [PubMed: 9248061]

Hull C, Isaacson JS, Scanziani M. Postsynaptic mechanisms govern the differential excitation of cortical neurons by thalamic inputs. J Neurosci. 2009; 29:9127–9136. [PubMed: 19605650]

Ichinose T, Fyk-Kolodziej B, Cohn J. Roles of ON cone bipolar cell subtypes in temporal coding in the mouse retina. J Neurosci. 2014; 34:8761–8771. [PubMed: 24966376]

Kerchner GA, Nicoll RA. Silent synapses and the emergence of a postsynaptic mechanism for LTP. Nat Rev Neurosci. 2008; 9:813–825. [PubMed: 18854855]

Kim JS, Greene MJ, Zlateski A, Lee K, Richardson M, Turaga SC, Purcaro M, Balkam M, Robinson A, Behabadi BF, et al. Space-time wiring specificity supports direction selectivity in the retina. Nature. 2014; 509:331–336. [PubMed: 24805243]

Krukowski AE, Miller KD. Thalamocortical NMDA conductances and intracortical inhibition can explain cortical temporal tuning. Nat Neurosci. 2001; 4:424–430. [PubMed: 11276234]

Lawrence JJ, McBain CJ. Interneuron diversity series: containing the detonation--feedforward inhibition in the CA3 hippocampus. Trends Neurosci. 2003; 26:631–640. [PubMed: 14585604]

Lee S, Chen L, Chen M, Ye M, Seal RP, Zhou ZJ. An unconventional glutamatergic circuit in the retina formed by vGluT3 amacrine cells. Neuron. 2014; 84:708–715. [PubMed: 25456497]

Lee S, Kim K, Zhou ZJ. Role of ACh-GABA cotransmission in detecting image motion and motion direction. Neuron. 2010; 68:1159–1172. [PubMed: 21172616]

Linaro D, Storace M, Giugliano M. Accurate and fast simulation of channel noise in conductance-based model neurons by diffusion approximation. PLoS Comput Biol. 2011; 7:e1001102. [PubMed: 21423712]

Lipin MY, Taylor WR, Smith RG. Inhibitory input to the direction-selective ganglion cell is saturated at low contrast. J Neurophysiol. 2015; 114:927–941. [PubMed: 26063782]

London M, Hausser M. Dendritic computation. Annu Rev Neurosci. 2005; 28:503–532. [PubMed: 16033324]

Maccaferri G, Toth K, McBain CJ. Target-specific expression of presynaptic mossy fiber plasticity. Science. 1998; 279:1368–1370. [PubMed: 9478900]

Manookin MB, Weick M, Stafford BK, Demb JB. NMDA receptor contributions to visual contrast coding. Neuron. 2010; 67:280–293. [PubMed: 20670835]

Mauss AS, Vlasits A, Borst A, Feller M. Visual Circuits for Direction Selectivity. Annu Rev Neurosci. 2017

Murphy BK, Miller KD. Multiplicative gain changes are induced by excitation or inhibition alone. J Neurosci. 2003; 23:10040–10051. [PubMed: 14602818]

Nowak P, Dobbins AC, Gawne TJ, Grzywacz NM, Amthor FR. Separability of stimulus parameter encoding by on-off directionally selective rabbit retinal ganglion cells. J Neurophysiol. 2011; 105:2083–2099. [PubMed: 21325684]

Odermatt B, Nikolaev A, Lagnado L. Encoding of luminance and contrast by linear and nonlinear synapses in the retina. Neuron. 2012; 73:758–773. [PubMed: 22365549]

Park SJ, Kim IJ, Looger LL, Demb JB, Borghuis BG. Excitatory synaptic inputs to mouse on-off direction-selective retinal ganglion cells lack direction tuning. J Neurosci. 2014; 34:3976–3981. [PubMed: 24623775]

Poleg-Polsky A, Diamond JS. NMDA Receptors Multiplicatively Scale Visual Signals and Enhance Directional Motion Discrimination in Retinal Ganglion Cells. Neuron. 2016a; 89:1277–1290. [PubMed: 26948896]

Poleg-Polsky A, Diamond JS. Retinal Circuitry Balances Contrast Tuning of Excitation and Inhibition to Enable Reliable Computation of Direction Selectivity. J Neurosci. 2016b; 36:5861–5876. [PubMed: 27225774]

Rivadulla C, Sharma J, Sur M. Specific roles of NMDA and AMPA receptors in direction-selective and spatial phase-selective responses in visual cortex. J Neurosci. 2001; 21:1710–1719. [PubMed: 11222660]

Rivlin-Etzion M, Zhou K, Wei W, Elstrott J, Nguyen PL, Barres BA, Huberman AD, Feller MB. Transgenic mice reveal unexpected diversity of on-off direction-selective retinal ganglion cell subtypes and brain structures involved in motion processing. J Neurosci. 2011; 31:8760–8769. [PubMed: 21677160]

Sagdullaev BT, McCall MA, Lukasiewicz PD. Presynaptic inhibition modulates spillover, creating distinct dynamic response ranges of sensory output. Neuron. 2006; 50:923–935. [PubMed: 16772173]

Schiller J, Major G, Koester HJ, Schiller Y. NMDA spikes in basal dendrites of cortical pyramidal neurons. Nature. 2000; 404:285–289. [PubMed: 10749211]

Self MW, Kooijmans RN, Super H, Lamme VA, Roelfsema PR. Different glutamate receptors convey feedforward and recurrent processing in macaque V1. Proc Natl Acad Sci U S A. 2012; 109:11031–11036. [PubMed: 22615394]

Sethuramanujam S, McLaughlin AJ, deRosenroll G, Hoggarth A, Schwab DJ, Awatramani GB. A Central Role for Mixed Acetylcholine/GABA Transmission in Direction Coding in the Retina. Neuron. 2016; 90:1243–1256. [PubMed: 27238865]

Shima K, Tanji J. Involvement of NMDA and non-NMDA receptors in the neuronal responses of the primary motor cortex to input from the supplementary motor area and somatosensory cortex: studies of task-performing monkeys. Jpn J Physiol. 1998; 48:275–290. [PubMed: 9757144]

Silver RA. Neuronal arithmetic. Nat Rev Neurosci. 2010; 11:474–489. [PubMed: 20531421]

Stafford BK, Park SJ, Wong KY, Demb JB. Developmental changes in NMDA receptor subunit composition at ON and OFF bipolar cell synapses onto direction-selective retinal ganglion cells. J Neurosci. 2014; 34:1942–1948. [PubMed: 24478373]

Stokes CC, Isaacson JS. From dendrite to soma: dynamic routing of inhibition by complementary interneuron microcircuits in olfactory cortex. Neuron. 2010; 67:452–465. [PubMed: 20696382]

Szapiro G, Barbour B. Multiple climbing fibers signal to molecular layer interneurons exclusively via glutamate spillover. Nat Neurosci. 2007; 10:735–742. [PubMed: 17515900]

Taylor WR, Vaney DI. Diverse synaptic mechanisms generate direction selectivity in the rabbit retina. J Neurosci. 2002; 22:7712–7720. [PubMed: 12196594]

Toth K, Suares G, Lawrence JJ, Philips-Tansey E, McBain CJ. Differential mechanisms of transmission at three types of mossy fiber synapse. J Neurosci. 2000; 20:8279–8289. [PubMed: 11069934]

Trenholm S, Johnson K, Li X, Smith RG, Awatramani GB. Parallel mechanisms encode direction in the retina. Neuron. 2011; 71:683–694. [PubMed: 21867884]

Trong PK, Rieke F. Origin of correlated activity between parasol retinal ganglion cells. Nat Neurosci. 2008; 11:1343–1351. [PubMed: 18820692]

Tukker JJ, Taylor WR, Smith RG. Direction selectivity in a model of the starburst amacrine cell. Vis Neurosci. 2004; 21:611–625. [PubMed: 15579224]

Vaney DI, Sivyer B, Taylor WR. Direction selectivity in the retina: symmetry and asymmetry in structure and function. Nat Rev Neurosci. 2012; 13:194–208. [PubMed: 22314444]

Wang XJ. Synaptic reverberation underlying mnemonic persistent activity. Trends Neurosci. 2001; 24:455–463. [PubMed: 11476885]

Yonehara K, Farrow K, Ghanem A, Hillier D, Balint K, Teixeira M, Juttner J, Noda M, Neve RL, Conzelmann KK, et al. The first stage of cardinal direction selectivity is localized to the dendrites of retinal ganglion cells. Neuron. 2013; 79:1078–1085. [PubMed: 23973208]

Yu WQ, Grzywacz NM, Lee EJ, Field GD. Cell-type specific changes in retinal ganglion cell function induced by rod death and cone reorganization in rats. J Neurophysiol. 2017 jn 00826 02016.

Yushkevich PA, Piven J, Hazlett HC, Smith RG, Ho S, Gee JC, Gerig G. User-guided 3D active contour segmentation of anatomical structures: significantly improved efficiency and reliability. Neuroimage. 2006; 31:1116–1128. [PubMed: 16545965]

Zhang J, Diamond JS. Subunit- and pathway-specific localization of NMDA receptors and scaffolding proteins at ganglion cell synapses in rat retina. J Neurosci. 2009; 29:4274–4286. [PubMed: 19339621]

Zylberberg J, Cafaro J, Turner MH, Shea-Brown E, Rieke F. Direction-Selective Circuits Shape Noise to Ensure a Precise Population Code. Neuron. 2016; 89:369–383. [PubMed: 26796691]

Zylberberg J, Cafaro J, Turner MH, Shea-Brown E, Rieke F. Direction-Selective Circuits Shape Noise to Ensure a Precise Population Code. Neuron. 2016; 89:369–383. [PubMed: 26796691]

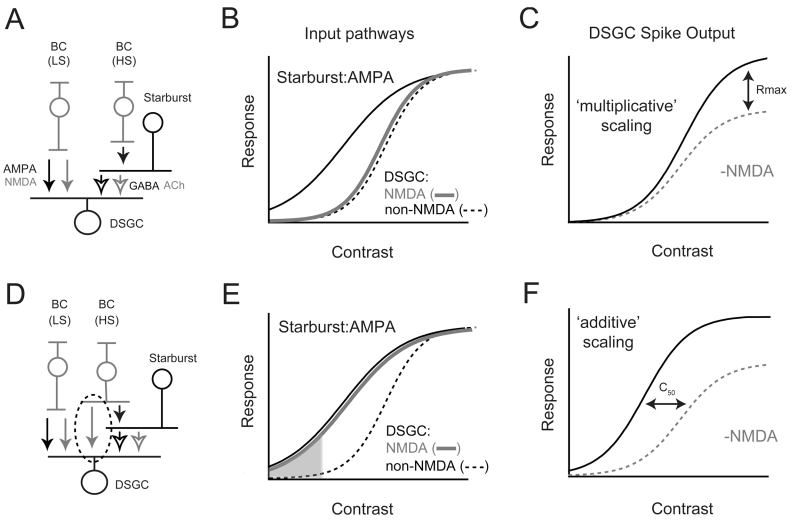

Figure 1. 'Matched' and 'silent synapse' models for E/I coordination in the DS circuit

A. Schematic of the 'matched' model for DS. High-sensitivity (HS) bipolar cells (BCs) drive starbursts, while low-sensitivity (LS) BCs drive DSGCs (Poleg-Polsky and Diamond, 2016b). HS-BCs drive starbursts via AMPA receptors while the LS-BCs drive DSGCs using both AMPA and NMDA receptors. The starbursts, themselves, drive DSGCs via $GABA_A$ and nicotinic Ach receptors (open arrows)

B. In the matched model, HS-BC inputs to starbursts are mediated by AMPA receptors. LS-BC input to DSGCs initiate precisely when starbursts reach their threshold for GABA/ ACh release. Thus, postsynaptic NMDA and non-NMDA (nACh/GABA/AMPA) receptor-mediated responses in DSGCs scale in proportion as a function of contrast (i.e. they are 'matched')

C. Multiplicative scaling: The matched model predicts that NMDA scales the DSGC spiking responses by a fixed fraction throughout its contrast range.

D. In the 'silent synapse' model to be tested here, common input provided by HS-BCs drive both starbursts and DSGCs (highlighted by the dashed circle). HS-BCs drive AMPA inputs in starbursts (black arrows), but NMDA-only inputs in DSGCs (grey arrows). Note, in both models presented (**A, D**) direction coding in DSGCs relies on asymmetric GABA release from starbursts (not depicted in the normalized contrast response functions).

E. In the silent synapse model, NMDA receptor-mediated inputs to DSGCs scale together with starburst inputs, while non-NMDA (ACh and AMPA) inputs initiate at a higher contrast. In this model, NMDA receptors are the only conductance activated in DSGCs at low-contrasts (shaded region). However, these NMDA receptors are silent until the DSGC receives non-NMDA inputs, a consequence of their voltage dependence (Sethuramanujam et al., 2016).

F. Additive scaling: The silent synapse model predicts that NMDA modulation of DSGC spiking would shift responses along the x-axis, increasing responses maximally in the middle of the contrast range.

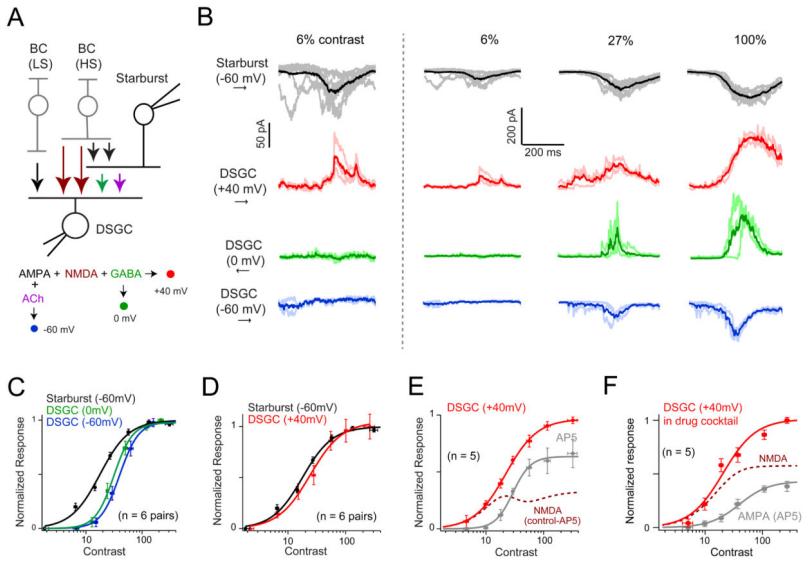

Figure 2. A high-sensitivity 'silent' NMDA receptor-mediated pathway to DSGCs

A. Schematic of the simultaneous starburst/DSGC paired recording configuration. The strategy used in voltage-clamp experiments to assess the contribution of different synaptic receptors is diagramed in the flowchart below. Specifically, DSGC were held at 0mV to isolate GABA (green); -60mV to isolate AMPA + ACh (blue); +40mV to isolate AMPA+ NMDA + GABA (red; note nACh receptors exhibit a strong inward rectification and do not contribute significantly to currents measured at +40 mV). The color scheme is used in all the panels in this figure.

B. Example traces depicting synaptic ON responses measured in starbursts and DSGCs evoked at three different contrasts (Weber contrast indicated on top). The darker traces indicate the average response, while the lighter traces illustrate the individual trials. The first column shows responses to 6% contrast at a higher magnification, illustrating that significant responses are only present at +40 mV in DSGCs, indicating the expression of 'silent' NMDA synapses. The voltage level at which DSGCs were clamped are indicated on the left. Synaptic responses were evoked by preferred-direction motion, except for inhibition, which was evoked by null-direction motion (indicated by arrows on the left). Threshold responses at +40 mV are non-directional, while threshold responses at 0 mV are highly directional (Figure S2).

C. Peak GABA and non-NMDA (ACh+AMPA) receptor-mediated synaptic inputs to DSGCs (mean ± SEM; n = 6 pairs) scale together as a function of stimulus contrast. These inputs have a relatively lower sensitivity compared to AMPA receptor-mediated inputs to starbursts (See Table 1 for comparisons on sensitivity). The solid lines indicate the Naka Rushton fit. Note all responses were centered to the starburst semi-saturating constant (see Figure S1; also see text for details).

D. The sensitivity of the synaptic responses measured in DSGCs at +40 mV is well matched to the sensitivity of synaptic inputs driving starbursts (mean ± SEM; n = 6 pairs). This is the first indication that DSCGs and starbursts are driven by common input.

E. NMDA receptor-mediated inputs to DSGCs are driven by a high-sensitive glutamate source. The average peak amplitude of the DSGC response measured at +40mV (mean ±

SEM) in control Ringer's solution (red), or in the added presence of an NMDA receptor antagonist (D- AP5; gray trace; n = 5). The dotted line indicates the NMDA receptor component (control-AP5).

F. NMDA and AMPA receptor-mediated inputs to DSGCs are driven by glutamate sources with different contrast sensitivities. DSGC responses were measured in a drug cocktail (10 μM SR- 95531, 100 μM hexamethonium and 10 μM UBP310) to isolate AMPA and NMDA receptor- mediated responses, or in the added presence of D-AP5 to isolate AMPA receptor responses (n = 5; mean ± SEM). Figure S3 illustrates the minimal effect of D-AP5 on starbursts responses recorded simultaneously.

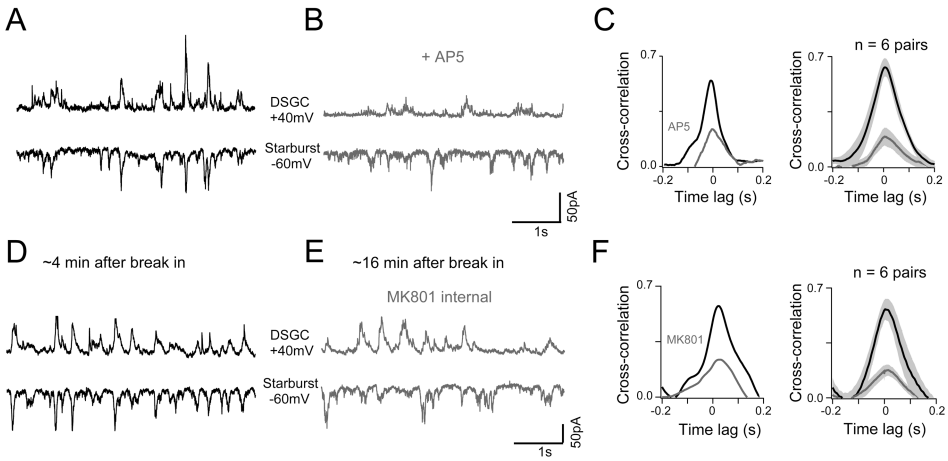

Figure 3. The NMDA receptor-mediated pathway to DSGCs is strongly shared with starbursts

A - B. Spontaneous AMPA/NMDA inputs measured simultaneously in a starburst and a neighboring DSGC in control Ringer's (**A**) or in the added presence of D-AP5 (**B**). Starbursts were held at -60mV and DSGCs at +40mV. AMPA/NMDA inputs were isolated in the cocktail of antagonists (SR-95531, hexamethonium, and UBP310).

C. A comparison of the cross-correlation function for activity in the pair shown in **A** and **B** (*left*), or population average (n = 6 pairs; *right*; mean ± SEM).

D - E. Spontaneous AMPA/NMDA inputs recorded in a starburst-DSGC pair with MK801 in the DSGC internal. **D** and **E** show the recording at 4 minutes and 16 minutes after break in respectively.

F. A comparison of the cross-correlation function for activity in the pair shown in **D** and **E** *(left).* The average cross-correlation function computed across 6 pairs measured during the early or late phases of the recording are illustrated in the right panel (mean ± SEM).

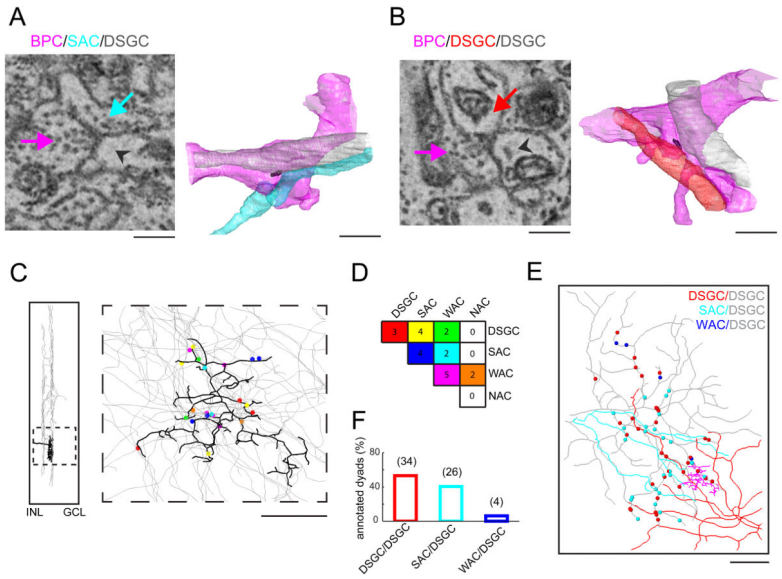

Figure 4. Anatomical evidence for common input to starbursts and DSCGs

A. Bipolar cells form dyads, where single presynaptic terminals activate post-synaptic receptors located on processes of different neurons. An example of a bipolar dyad contacting a starburst amacrine cell (SAC) and a DSGC *(left)* is illustrated. The arrows point to the bipolar cell ribbon (pink), the starburst process (turquoise) or the DSGC process (gray arrowhead). The ribbon can be identified by a faint gray sheet surrounded by a halo of vesicles (rather than an intense electron dense structure seen in post-stained serial sections). A 3D reconstruction of the same dyad (*right*; color-coded as in *left*); the 3D ribbon reconstruction itself is shown in black. Scale bar = 1μm.

B. An example dyad contacting two DSGCs.

C. Reconstruction of a bipolar terminal identified from its dyadic contact with a DSGC. The thick dendritic stratification of the terminal in the inner plexiform layer was characteristic of the type 5t bipolar cell (*left*). A total of 22 ribbon synapses were identified in this terminal. Subsequently, the two processes in these dyads were reconstructed to identify postsynaptic partners, including: DSGCs, starbursts (SAC), wide-field amacrine cells (WACs) and narrow- field amacrine cells (NACs). Scale bar = 10 μm.

D. The frequency of the bipolar cell contacts with 4 cell types (DSGCs, starbursts, WACs and NACs) is shown in the matrix. The combinations are color-coded as indicated in **C**.

E. Alternatively, dyadic connections (n=64; ~ 20-30 bipolar cells) were identified on the ON endritic tree of a DSGC (gray), from which the second postsynaptic process was traced. Dyads on the reconstructed DSGC dendritic tree (gray) color-coded according to the second dyadic partner; another DSGC (red), starburst (cyan) or wide-field amacrine cell (blue). Scale bar = 25μm.

F. Fraction of DSGC, starburst or wide-field processes that are shared with dyads contacting a single DSGC (grey cell in **E**).

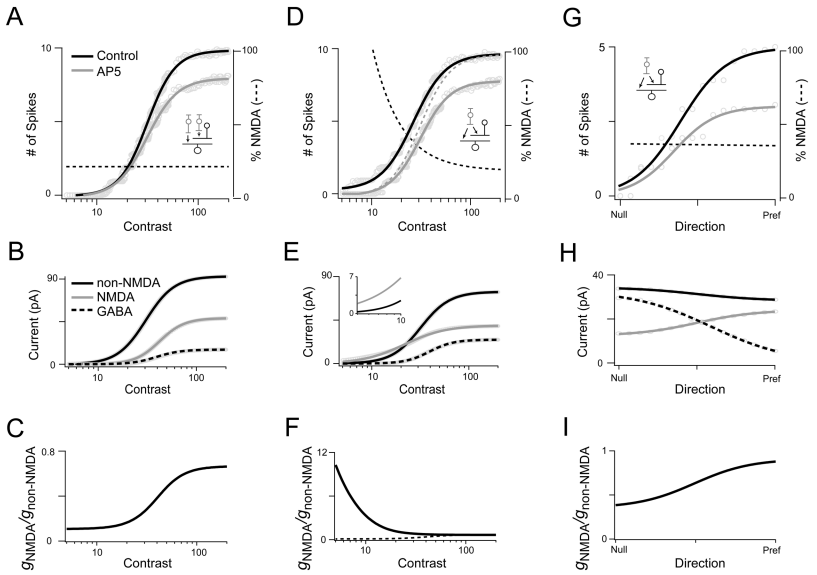

Figure 5. A simplified two-compartment computational model predicts that NMDA receptors transform DSGC responses using distinct 'arithmetical' operations

A. Spike output of a two-compartmental neuron model driven by non-NMDA, NMDA and GABA inputs scaling together with contrast (inset depicts the matched model; see Figure 1A for details) in control (black), and AP5 (grey; simulated by not including NMDA input in the model). The spiking response averaged over 20 trials was fit to the Naka-Rushton equation. The dashed line indicates the relative NMDA contribution to spike activity (% blocked by AP5), which was constant across contrasts, indicating multiplicative scaling by NMDA receptors.

B. The average amplitude of non-NMDA, NMDA and GABA currents generating the 'control' response shown in **A**.

C. The relative NMDA conductance ($G_{NMDA}/G_{non\text{-}NMDA}$) generating the 'control' response in **A,** is plotted against contrast.

D. Similar to **A**, except NMDA input was shifted relative to the non-NMDA inputs according to our experimental measurements (simulating the silent synapse model shown in the inset; see Figure 2E for details). The relative NMDA contribution to spike activity is maximal at the lowest contrasts (dashed black line). Relative responses less than 10% of the maximum were dominated by noise and were therefore omitted. The dotted gray line provides an indication of the response predicted by multiplicative scaling.

E - F. The non-NMDA, NMDA and GABA currents, and relative NMDA/non-NMDA conductances generating the control responses are shown in **E** and **F**, respectively. The *inset* in **E** shows an expanded view of the low-contrast range where NMDA currents dominate. In **F**, the NMDA/non-NMDA conductance ratio from **C** (dotted line) is shown for comparison.

G. Responses in a silent synapse model neuron driven by non-directional non-NMDA/NMDA input but strongly directional GABA input, in control conditions or in the presence of AP5. Spiking responses to 16 directions (between null- and preferred -directions), averaged over 20 trials were fitted with a sigmoid equation (solid lines). The dashed line indicates the relatively fixed contribution of NMDA receptors to the spike activity across direction, indicative of a multiplicative scaling operation. This property is reliant on the

voltage dependence of NMDA receptors (Figure S4; also see (Poleg-Polsky and Diamond, 2016b)).

H - I. The non-NMDA, NMDA and GABA receptor-mediated currents, and relative NMDA/non-NMDA conductances generating the control responses are shown in **H** and **I**, respectively.

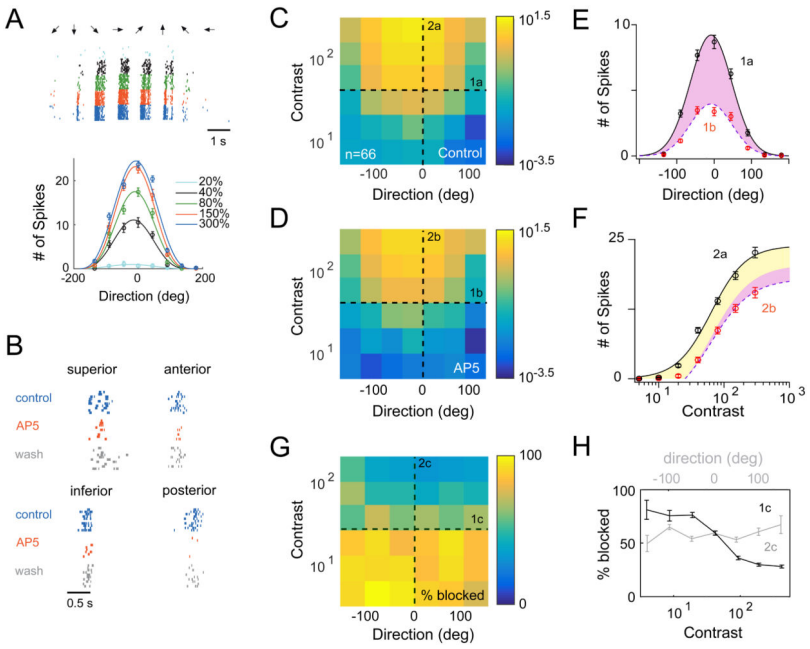

Figure 6. Additive and multiplicative scaling operations mediated by NMDA receptors

A. An example DSGC response recorded on a multi-electrode array. Spikes were evoked by drifting bars (240 μm wide on the retina, moving at 960 μm/s; 8 directions, 7 contrasts indicated by different colors; 10 trials for each contrast). ON-OFF DSGCs were distinguished from other ganglion cells based on their tuning properties: see Figure S5). The bottom plot shows the tuning curves of this DSGC plotted for multiple contrasts (mean ± SEM). Responses at each contrast were fit with a cosine function.

B. NMDA receptor antagonist, 50 μM D-AP5, reversibly reduced responses (preferred motion; 20-40% contrast) to a similar extent in the four subtypes of ON-OFF DSGCs.

C. A heat map of the population DSGC response as a function of direction and contrast measured in control conditions (the color bar indicates the average number of spikes/trial on a logarithmic scale). Responses were averaged across the four types of ON-OFF DSGCs (21 superior, 12 inferior, 27 anterior, and 6 posterior-coding DSGCs).

D. Same as **C**, except responses were measured in the presence of D-AP5.

E. Cross-sections of the heat maps along the direction axis, in control and in D-AP5 (1a from **C**; 1b from **D**). The solid line indicates the Gaussian fit of the control data (black circles). The same Gaussian fit could be scaled to approximate the response measured in D-AP5 (red circles; purple shaded region indicates the D-AP5-sensitive component that could be accounted for by multiplicative scaling; See Figure S6). Data are represented as mean ± SEM.

F. Cross-sections of the heat maps along the contrast axis, in control and in D-AP5 (2a from **C**; 2b from **D**) for preferred direction stimuli. The control response (black circles) was fit with the hyperbolic Naka-Rushton Equation (solid line; see methods). The response measured in D-AP5 (red circles) could be approximated by scaling the control response in the Y-dimension as depicted by the dashed line (purple and yellow shaded regions indicate the D-AP5-sensitive component that could be accounted for by purely multiplicative or additive scaling operations, respectively) (Figure S6 illustrates how these scaling factors

were determined). D-AP5 did not affect the responses of ON transient ganglion cells (see Figure S5), which was used as an indicator of the stability of contrast sensitivity of the retina for the duration of the experiment. Data are represented as mean ± SEM.

G. A heat map indicating the relative suppression of responses by D-AP5 across contrasts and direction (scale bar represents % suppression; (Control-AP5)/Control*100).

H. Cross-sections of the heat maps along the direction (grey; 1c from **G**) and contrast axes (black; 1c from **G**). The fraction of the response blocked by D-AP5 did not systematically change with direction, but varied strongly with contrast. Data are represented as mean ± SEM.

Table M1

Parameter		
	Soma	**Dendrite**
Diameter	10 μm	1 μm
Length	10 μm	200 μm
Ra	100 Ω cm	100 Ω cm
cm	1 μf/cm	1 μf/cm
6gleak/g_pas	0.0001667 S/cm^2	0.0001667 S/cm^2
eleak/e_pas	-60 mV	-60 mV
gkbar	0.07 S/cm^2	---
gnabar	0.24 S/cm^2	---
gkmbar	0.003 S/cm^2	---
HHst noise	0.5	---

Table M2

Naka-Rushton fits $g = g_{max}*(C^n/(C^n+C_{50}^n))$			
	C_{50} (SAC C_{50} = 17)	n	g_{max} (nS)
E	42.5	2.99	1.5
Low-sensitive NMDA	42.5	2.99	6
High-sensitive NMDA	8.8	1.81	6
Preferred I	30.0	2.853	4
Null I	30.0	2.853	35